mathematics

MDPI

Article

Effect of an Applied Magnetic Field on Joule Heating-Induced Thermal Convection

Anupam M. Hiremath [1], Harunori N. Yoshikawa [2,3] and Innocent Mutabazi [1,*]

[1] Université Le Havre Normandie, Normandie Université, LOMC CNRS UMR 6294, 76058 Le Havre, France; anupam-mahantayya.hiremath@etu.univ-lehavre.fr
[2] Faculty of Science and Engineering, Doshisha University, Kyoto 602-0321, Japan; hayoshik@mail.doshisha.ac.jp
[3] Université de Côte d'Azur, INPHYNI CNRS UMR 7010, 06100 Nice, France
* Correspondence: innocent.mutabazi@univ-lehavre.fr

Abstract: Thermal convection induced by internal heating appears in different natural situations and technological applications with different internal sources of heat (e.g. radiation, electric or magnetic fields, chemical reactions). Thermal convection due to Joule heating in weak electrical conducting liquids such as molten salts with symmetric thermal boundary conditions is investigated using linear stability analysis. We show that, in the quasi-static approximation where the induced magnetic field is negligible, the effect of the external magnetic field consists of the delay in the threshold of thermal convection and the increase in the size of thermoconvective rolls for an intense magnetic field. Analysis of the budget of the perturbations' kinetic energy reveals that the Lorentz force contributes to the dissipation of the kinetic energy.

Keywords: thermal convection; Joule heating; Chebyshev polynomials; collocation method; Lorentz force

MSC: 80; 76

check for updates

Citation: Hiremath, A.M.; Yoshikawa, H.N.; Mutabazi, I. Effect of an Applied Magnetic Field on Joule Heating-Induced Thermal Convection. *Mathematics* **2024**, *12*, 3395. https://doi.org/10.3390/math12213395

Academic Editor: Ilya Simanovskii

Received: 5 September 2024
Revised: 16 October 2024
Accepted: 18 October 2024
Published: 30 October 2024

Copyright: © 2024 by the authors. Licensee MDPI, Basel, Switzerland. This article is an open access article distributed under the terms and conditions of the Creative Commons Attribution (CC BY) license (https://creativecommons.org/licenses/by/4.0/).

1. Introduction

Recent technological developments in metallurgy include the design of concentrated solar panels associated with thermal energy storage and in nuclear engineering where molten salt reactors appear to be a promising issue [1–6], have increased the demand for efficient heat exchangers that can operate at very high temperatures. For high-temperature operations, most of the fluids tend to evaporate or might need a huge amount of pressure to increase their boiling points. One method to overcome these challenges is the utilization of molten salts. Solid at room temperature, salts cannot transfer heat by convection and hence they need to be preheated above their melting point but kept under the boiling point in order to produce convective motion inside them. Due to their large thermal capacity and higher boiling points, molten salts are widely employed for thermal transfer at high temperatures and in recent applications, they are used as electrolytes for energy storage systems such as liquid metal battery [7–10].

Salts are typically inorganic ionic mixtures of fluorides, chlorides, carbonates, etc. Depending on the application, molten salts can be made of binary such as LiCl, or ternary molecules such as NaCl-NaI. Due to the strong ionic bonds between the atoms, a huge amount of heat is required to bring them to a liquid state. Hence, molten salts need to be maintained at high temperatures to keep them in a stable liquid state. Due to their low electrical and thermal conductivities, the application of an electrical current generates the Joule heating in the molten salts. This internal heating can trigger thermal convective motions in the molten salts and modify the heat transfer coefficient with their container.

Thermal convection induced by internal heating has been investigated by many authors [11–22] because this phenomenon is encountered in many engineering situations where internal heating can be induced by viscous heating or by dielectric heating or any other localized internal heat sources. It occurs also in Earth's mantle where convective motions are sustained by radiogenic heating throughout the mantle itself and by the conduction from the underlying hot outer core due to internal radiation. In the upper atmosphere, thermal convection is driven by radiative cooling and by heating from the lower atmosphere and the Earth's surface [14]. In an astrophysical context, nuclear burning processes occur in thin shells at some distance from the center of the star leading to compressible thermoconvective motions in the star [17]. Molten salts are also used as electrolytes between electrodes in thermal batteries used in military applications for guided missiles but also as primary power sources for radar and electronic packages for nuclear weapons [21] However, convection induced by internal heating has received much less attention than Rayleigh–Bénard convection induced by a constant temperature gradient imposed at the plates bounding the fluids [23,24].

The conduction state induced by internal heating has a parabolic temperature profile compared to the linear profile of the conduction state induced by fixed temperature difference. Linear stability analysis has been performed by different authors using different kinematic and thermal boundary conditions [11–13,17] to predict the threshold of thermal convection induced by internal heating. Numerical simulations have been performed to estimate the hydrodynamic field and the heat transfer coefficient associated with internal heating [14–16]. Sparrow et al. [11] were the first to tackle the problem of thermal convection induced by internal heating in a fluid between two parallel plates with different thermal boundary conditions, using a semi-analytical method. They found that the threshold of thermal convection decreases with the magnitude of the internal heat source. The same problem was revisited by Kulaki et al. [12,13] who performed a more exhaustive linear stability analysis and energetic analysis and obtained more accurate results on the critical parameters of thermal convection induced by internal heating. The implication of internal heating in the astrophysical environment and in geophysics was developed by Strauss [17] and by Goluskin et al. [14]. Another type of internal heating induced by a high-frequency electric field in dielectric liquids under microgravity conditions was investigated by Yoshikawa et al. [18] who showed also that the temperature of the conducting state has a parabolic profile and determined the critical parameters for thermo-electro-convection induced by the dielectrophoretic buoyancy force. Thermal convection induced by Joule-heating from magnetic fields has also been investigated in more complex flow systems such as generalized Couette flow of Jeffrey fluid [19] or in a cylindrical annulus with different magnetic configurations [20]. The estimate of convective flows and heat transfer induced by internal heating was performed in direct numerical simulations by Goluskin et al. [14,16]. A recent work by Wang et al. [25] developed the unifying theory of scaling laws of turbulence in thermal convection induced by internal heating. All these studies have confirmed that, due to the parabolic temperature profile of the conduction state, thermal convection induced by internal heating appears for lower value of the Rayleigh number compared to the threshold of Rayleigh–Bénard convection induced by an imposed constant temperature gradient.

In most geophysical and astrophysical situations but also in technological applications, the magnetic field has a strong impact on the thermal convection in fluids. The effect of the magnetic field on Rayleigh–Bénard convection has been theoretically predicted by Chandrasekhar [23] who showed the delay of the threshold of thermal convection in a liquid layer under a magnetic field. This effect has been confirmed by further studies on higher regimes of thermoconvection [26]. However, to our best knowledge, for internal heating-induced convection in a horizontal liquid layer, the effect of the magnetic field has received less attention if any.

We have performed linear stability analysis to investigate the effect of magnetic field on the thermal convection induced by Joule heating in an electrolyte-type liquid crossed by

a stationary homogeneous current for different kinematic and thermal boundary conditions. We have performed the energetic budget to identify the contribution of each force in the temporal evolution of the kinetic energy of perturbations close to the onset and we found that the Lorentz force acts as a dissipative force and delays the threshold to thermal convection induced by internal heating.

The paper is organized as follows. In Section 2, we formulate the problem of thermal convection induced by Joule heating. The results of the linear stability are presented in Section 3 and discussed in Section 4. The last Section consists of the Conclusion.

2. Problem Formulation

We consider a liquid layer of poor electrical and thermal conductivities, confined between two infinite horizontal plates located at $z = \pm d/2$ in a Cartesian coordinates system (Figure 1). The liquid is considered as incompressible and Newtonian with the density ρ, the thermal expansion coefficient α, the kinematic viscosity ν, the specific heat capacity c_p, the thermal conductivity $\lambda = \rho c_p \kappa$ (where κ is the thermal diffusivity) and the electrical conductivity σ.

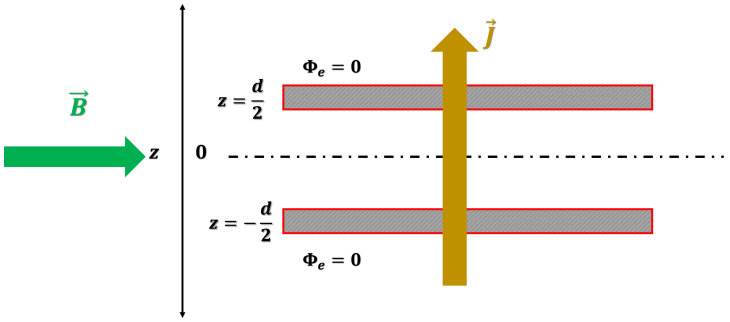


Figure 1. Liquid layer between two electrically conducting plates ($\Phi_e = 0$) located at $z = \pm d/2$ where Φ_e is the electric potential.

A uniform current I of density $\vec{J} = (I/S)\vec{e}_z$ applied across the fluid layer (of cross-section area S) generates a Joule heat in the liquid because of its weak electrical conductivity. The density q of the Joule heat flux across the liquid layer is

$$q = \frac{J^2}{\sigma} \tag{1}$$

2.1. Conduction State Induced by Internal Joule Heating

The stationary conduction state induced by Joule heating in a liquid layer confined between two horizontal infinite plates is characterized by the temperature profile $T(z)$ which satisfies the following heat equation

$$\frac{d^2T}{dz^2} + \frac{J^2}{\lambda\sigma} = 0 \tag{2}$$

To allow the heat exchange with the environment, we impose the Robin boundary conditions which are hybrid thermal boundary conditions combining both the Neumann and the Dirichlet conditions at the plates:

$$\begin{cases} \dfrac{dT}{dz} = -h(T - T_\infty) & \text{at } z = \dfrac{d}{2} \quad (3a) \\ \dfrac{dT}{dz} = h(T - T_\infty) & \text{at } z = -\dfrac{d}{2} \quad (3b) \end{cases}$$

where h is the heat exchange coefficient which incorporates both the convective and radiative heat transfer and T_∞ is the temperature in the bulk of the environment away

from the plates. Choosing d and ΔT as characteristic length and temperature, respectively, (i.e., $z = d\,z'$, $T - T_\infty = \Delta T\,\Theta$), the Joule heating yields the temperature scale $\Delta T = J^2 d^2/\lambda\sigma$. The stationary heat equation and the Robin boundary conditions in dimensionless form become

$$\begin{cases} \dfrac{d^2\Theta}{dz^2} + 1 = 0 & \text{(4a)} \\ \dfrac{d\Theta}{dz} = -Bi\,\Theta \qquad \text{at } z = \dfrac{1}{2} & \text{(4b)} \\ \dfrac{d\Theta}{dz} = Bi\,\Theta \qquad \text{at } z = -\dfrac{1}{2} & \text{(4c)} \end{cases}$$

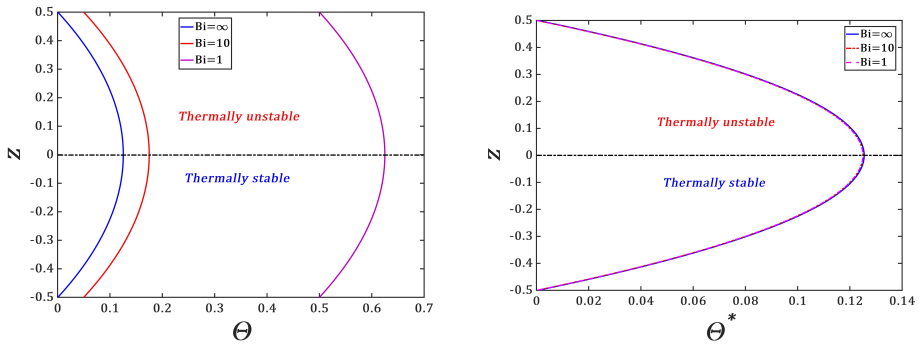
where $Bi = hd/k$ is called Biot number. From now, z is the dimensionless vertical coordinate. The conducting state induced by Joule heating in the liquid layer is thus described by a symmetric quadratic temperature profile

$$\Theta(z) = -\frac{1}{2}\left(z^2 - \frac{1}{4} - \frac{1}{Bi}\right) \tag{5}$$

The maximum temperature $\Theta_{max} = 1/(2Bi)$ is reached at the mid-plane $z = 0$ of the liquid layer and it is very sensitive to the heat exchange coefficient, i.e., to Bi [13]. For isothermal boundary conditions (Neumann conditions), i.e., for $Bi \to \infty$, we recover the temperature profile already obtained in previous studies [13,14]. The temperature profiles of the conducting state induced by the Joule heating are plotted in Figure 2. They differ from each other by the quantity Θ_{max} and they can be represented by a single curve $\Theta^*(z)$ (Figure 2b) defined as

$$\Theta^*(z) = \Theta(z) - \Theta_{max} \tag{6}$$

The symmetry of the temperature profiles with respect to the mid-plane of the liquid layer is due to the boundary conditions where the heat exchange coefficients between the plates bounding the liquid with the bulk environment are assumed to be identical. If they are different, the symmetry of the conduction state is broken, and the temperature profiles are asymmetric with coefficients containing the Biot numbers Bi_l of each plate l ($l = 1$: lower plate, $l = 2$: upper plate).



(**a**) (**b**)

Figure 2. Temperature profiles of the conduction state in Joule heated liquid with Robin boundary condition: (**a**) for different values of Bi. (**b**) for the scaled conduction state Θ^* where all the considered boundary conditions merge into a single curve.

2.2. Driving Forces and Control Parameters

The internal Joule heating induces a temperature gradient and thus the Archimedean buoyancy $\Delta\rho g (= -\alpha\Delta T\rho_0 g)$ within the liquid layer where ρ_0 is the liquid density at the reference temperature T_0. The lower layer of the liquid is thermally stable while the upper one is thermally unstable. We need to estimate the magnitude of the internal heating,

i.e., the magnitude of the applied current required to trigger thermal convection in the liquid layer. The Archimedean buoyancy will overcome the thermal diffusion and viscous dissipation if the Archimedean time scale τ_A is much smaller than the combined visco-diffusive timescale $\sqrt{\tau_\nu \tau_\kappa}$ in the liquid. The Archimedean timescale for a buoyant liquid particle to rise the distance $d/2$ is $\tau_A = \sqrt{d/[2g\alpha(\Delta T)_{max}]}$. The timescales for viscous dissipation and thermal diffusion of the buoyant particle which rises the same distance $d/2$ are $\tau_\nu = d^2/4\nu$ and $\tau_\kappa = d^2/4\kappa$, respectively. The temperature profile Θ^* in Figure 2b yields $(\Delta T)_{max} = \Delta T/8$. Thus, the magnitude of the Archimedean buoyancy can be estimated by the Rayleigh number defined as follows

$$Ra = \frac{\tau_\nu \tau_\kappa}{\tau_A^2} = \frac{1}{64}\frac{\alpha g J_0^2 d^5}{\rho c_p \nu \kappa^2 \sigma} = GrPr \tag{7}$$

where $Pr = \nu/\kappa$ is the Prandtl number and $Gr = U_{th}\, d/\nu$ is the Grashof number sometimes called the thermal Reynolds number if the characteristic thermal velocity of the buoyant particle under the action of Joule heating is introduced:

$$U_{th} = \frac{1}{64}\frac{\alpha g J_0^2 d^4}{\rho c_p \kappa \nu \sigma} \tag{8}$$

The second driving force in a liquid layer crossed by an electric current density $\vec{J}$ and an applied horizontal magnetic field $\vec{B}$ is the Lorentz force density $\vec{F} = \vec{J} \times \vec{B}$. For weakly electrically conducting liquids $\sigma \approx \mathcal{O}(10^2)$ S/m and for thermal convective velocities at laboratory scales $V \approx \mathcal{O}(10^{-2})$ m/s, the magnetic fields induced by the current density $\vec{J}$ and the drift Maxwell current $\vec{J}_d = \mu\epsilon\partial D/\partial t$ due to time variations of the electric field are so weak that they can be neglected in the so-called "quasi-static approximation" [27]. Here, μ and ϵ represent the magnetic permeability and the electrical permittivity of the liquid. The electric field $\vec{E}$ is thus stationary and it can be written as $\vec{E} = -\vec{\nabla}\Phi_e$ where Φ_e is the electric potential chosen to vanish at the bounding plates at $z = \pm d/2$ (Figure 1). The density current in the liquid is given by Ohm law

$$\vec{J} = \sigma\left(\vec{E} + \vec{u} \times \vec{B}\right) \tag{9}$$

where $\vec{u}$ is the velocity induced in the liquid. The stationarity of the applied current density $\left(\vec{\nabla}.\vec{J} = 0\right)$ leads to the Poisson equation relating the electric potential to the magnetic field:

$$\Delta\Phi_e = \nabla.\left(\vec{u} \times \vec{B}\right) \tag{10}$$

In the quasi-stationary approximation [27], the electric field in the conducting state is homogeneous and the electric potential satisfies the Laplace equation: $\nabla^2\Phi_e = 0$. This means that the electric field between the plates is homogeneous. The Ohm law becomes

$$\vec{J} = \sigma\left(-\vec{\nabla}\Phi_e + \vec{u} \times \vec{B}\right) \tag{11}$$

To estimate the magnitude of the Lorentz force acting in the liquid, we introduce the Hartmann number Ha which is the ratio of the magnitude B_0 of the applied magnetic field to the intrinsic magnetic field of the liquid B_i

$$Ha = \frac{B_0}{B_i} \;,\; B_i = \frac{1}{d}\sqrt{\frac{\rho\nu}{\sigma}} \tag{12}$$

The Hartmann number is often defined as the ratio between the characteristic length of the flow d and the Hartmann length l_{Ha}, i.e.,

$$Ha = \frac{d}{l_{Ha}} \ , \ l_{Ha} = \frac{1}{B_0}\sqrt{\frac{\sigma}{\rho\nu}} \tag{13}$$

The quantity $Q = Ha^2$ is called the Chandrasekhar number.

To make the governing equations dimensionless, we use the liquid layer thickness d as the characteristic scale for space coordinates, i.e., $\vec{r} = d\,\vec{\tilde{r}}$ and the viscous diffusion velocity $d/\tau_\nu = \nu/d$ as a characteristic velocity, i.e., $\vec{u} = (\nu/d)\,\vec{\tilde{u}}$ because we have chosen the viscous time as the characteristic timescale, i.e., $t = \tau_\nu\,\tilde{t}$. The dynamics of the liquid subject to Joule heating can be uniquely determined by four independent dimensionless control parameters given in Table 1. The Biot number Bi characterizes the heat exchange between the liquid and its environment, the Prandtl number Pr determines the thermo-viscous diffusive nature of the liquid, the Rayleigh number Ra measures the magnitude of the Archimedean buoyancy compared to the viscous dissipation and thermal diffusion, the Hartmann number Ha is the ratio between the Lorentz force and the viscous dissipation. The Grashoff number Gr is not an independent control parameter, it is sometimes used instead of Ra.

Table 1. List of independent control parameters.

Control Parameters	Symbol
Biot umber	Bi
Prandtl number	Pr
Rayleigh number	$Ra = GrPr$
Hartmann number	Ha

2.3. Linearized Equations for Internal Heating-Driven Convection

As of now, all variables are dimensionless, for simplicity, we have dropped the tildes above variables $t, \vec{u}, \vec{r}$. We superimpose to the conduction state small perturbations of the temperature field θ', of the electric potential Φ', of the generalized pressure H' and the velocity $\vec{u} = (u, v, w)$. We assume the validity of the Boussinesq approximation. Linearization of the momentum, energy and electric potential equations near the base state yield the following equations in non-dimensional form [7,27]:

$$\begin{cases} \vec{\nabla}.\vec{u} = 0 & \text{(14a)} \\ \dfrac{\partial \vec{u}}{\partial t} = -\vec{\nabla}H' + \sqrt{\dfrac{Pr}{Ra}}\Delta\vec{u} + \theta'\vec{e_z} \\ \qquad\qquad + Ha^2\sqrt{\dfrac{Pr}{Ra}}\left[\left(-\nabla\Phi' + \vec{u}\times\vec{B}\right)\times\vec{B}\right] & \text{(14b)} \\ \dfrac{\partial\theta'}{\partial t} + w\dfrac{d\Theta}{dz} = \dfrac{1}{\sqrt{Ra.Pr}}\Delta\theta' & \text{(14c)} \\ \Delta\Phi' = \nabla.\left(\vec{u}\times\vec{B}\right) & \text{(14d)} \end{cases}$$

The second term in Equation (14b) is due to the viscous dissipation, the third term is the Archimedean buoyancy and the last term represents the Lorentz force. The temperature field is coupled to the velocity field via Equation (14b) and Equation (14c). In the quasi-stationary approximation, the perturbation $\vec{b}$ of the magnetic field is neglected [27].

Two different kinematic boundary conditions are imposed on the fluid, i.e., the no-slip boundary condition where the velocity perturbations vanish at the walls and the free-slip

boundary condition where the normal stress vanishes at the walls. The free-slip boundary conditions read

$$\frac{\partial u}{\partial z} = \frac{\partial v}{\partial z} = w = \Phi' = 0 \qquad \text{at } z = \frac{1}{2}, -\frac{1}{2} \tag{15}$$

The no-slip boundary conditions are

$$u = v = w = \Phi' = 0 \qquad \text{at } z = \frac{1}{2}, -\frac{1}{2} \tag{16}$$

The thermal boundary conditions stem from boundary conditions (3):

$$\begin{cases} \dfrac{\partial \theta'}{\partial z} = -Bi\,\theta' & \text{at } z = \dfrac{1}{2} \quad (17a) \\ \dfrac{\partial \theta'}{\partial z} = Bi\,\theta' & \text{at } z = -\dfrac{1}{2} \quad (17b) \end{cases}$$

2.4. Normal Mode Expansion and Numerical Method

In the present study, we choose the horizontal axes in such a way that the magnetic field is applied along the horizontal axis $\vec{e}_x$ and its non-dimensional form is $\vec{B} = (1, 0, 0)$. The infinitesimal perturbations $\vec{\Psi}(t, x, y, z) = (u', v', w', H', \theta', \Phi')^t$ are expanded as normal modes

$$\vec{\Psi}(t, x, y, z) = \vec{\hat{\Psi}}(z) e^{st + i(k_x x + k_y y)} \tag{18}$$

where $\vec{\hat{\Psi}}(z) = \left(\hat{u}(z), \hat{v}(z), \hat{w}(z), \hat{H}(z), \hat{\theta}(z), \hat{\Phi}(z)\right)^t$ is the structure-function of the perturbations, the quantity $s = s_r + is_i$ is a complex temporal growth rate with s_r and s_i being the real growth rate and the frequency of the perturbations, respectively. As the system is assumed infinite in the horizontal plane, the wave numbers k_x and k_y are real. Substitution into the linearized Equation (14) yields the following system of equations of the complex amplitudes $\vec{\hat{\Psi}}$:

$$\begin{cases} 0 = ik_x\hat{u} + ik_y\hat{v} + D\hat{w} & (19a) \\ s\hat{u} = -ik_x\hat{H} + \sqrt{\dfrac{Pr}{Ra}}\hat{\Delta}\hat{u} & (19b) \\ s\hat{v} = -ik_y\hat{H} + \sqrt{\dfrac{Pr}{Ra}}\hat{\Delta}\hat{v} - Ha^2\sqrt{\dfrac{Pr}{Ra}}\left[D\hat{\Phi} + \hat{v}\right] & (19c) \\ s\hat{w} = -D\hat{H} + \sqrt{\dfrac{Pr}{Ra}}\hat{\Delta}\hat{w} + \hat{\theta} + Ha^2\sqrt{\dfrac{Pr}{Ra}}\left[ik_y\hat{\Phi} - \hat{w}\right] & (19d) \\ s\hat{\theta} = -\hat{w}D\Theta + \dfrac{1}{\sqrt{Ra.Pr}}\hat{\Delta}\hat{\theta} & (19e) \\ 0 = \hat{\Delta}\hat{\Phi} + D\hat{v} - ik_y\hat{w} & (19f) \end{cases}$$

with the operators $D = \frac{d}{dz}, \hat{\Delta} = k_x^2 + k_y^2 + D^2$. The boundary conditions develops into,

$$\begin{cases} \text{No-slip boundary conditions :} & (20a) \\ \qquad \hat{u} = \hat{v} = \hat{w} = \hat{\Phi} = 0 \qquad \text{at } z = \dfrac{1}{2}, -\dfrac{1}{2} & \\ \text{Free-slip boundary conditions :} & (20b) \\ \qquad D\hat{u} = D\hat{v} = \hat{w} = \hat{\Phi} = 0 \qquad \text{at } z = \dfrac{1}{2}, -\dfrac{1}{2} & \\ \text{Thermal boundary conditions :} & (20c) \\ \qquad D\hat{\theta} = -Bi\,\hat{\theta} \qquad \text{at } z = \dfrac{1}{2} \text{ and } D\hat{\theta} = Bi\,\hat{\theta} \qquad \text{at } z = -\dfrac{1}{2} & \end{cases}$$

Besides the four control parameters given in Table 1, the system of linearized Equation (19) together with the boundary conditions (20) contains 10 dimensionless variables. The system of Equation (14) can be written in a matrix form as follows :

$$\overline{\overline{A}}\vec{\Psi} = s\overline{\overline{B}}\vec{\Psi} \tag{21}$$

where the expressions of the matrices $\overline{\overline{A}}$ and $\overline{\overline{B}}$ can easily be derived from the system of Equation (19). The system of Equation (21) is an eigenvalue problem with the eigenvalue s and the structure-function of the perturbations $\vec{\Psi}$ is the eigenvector. The eigenvalue s is searched as a function of the control parameters and of the wave numbers of the perturbations

$$s = f\left(Ra, Pr, Ha, k_x, k_y\right) \tag{22}$$

We are interested in the determination of the threshold of thermal convection, so we look for marginal perturbations for which $s_r = 0$. The marginal state is thus represented by the hypersurface $f(Ra, Pr, Ha, k_x, k_y, s_i) = 0$. We fix Pr and Ha and the hypersurface is reduced to a marginal stability curve $\tilde{f}(Ra, k) = 0$ for stationary perturbations where $k = \sqrt{k_x^2 + k_y^2}$.

In order to determine the marginal stability curve, we use the following numerical scheme. The system of equations of complex amplitudes (19) and the boundary conditions (20) are discretized using the Chebyshev spectral method. The Chebyshev variable ξ is related to the vertical coordinate z as follows,

$$\xi = 2z \tag{23}$$

where $\xi \in [-1, 1]$. Discretization is conducted along a vertical direction $z = z_i (i = 3, 4, 5, ..., N)$ corresponding to collocation points $\xi_i = \cos(i\pi/N)$. The highest order of Chebyshev polynomials is needed to ensure the convergence is set to $N = 60$.

Marginal stability curves for which $s_r = 0$ are plotted in the plane (k, Ra) and their lowest minimum determines the critical parameters (k_c, Ra_c) of thermal convection.

3. Results

In the absence of the magnetic field, the critical modes are invariant with respect to rotation of the wavenumber vector $\vec{k}$ in the plane (k_x, k_y): the critical patterns can either be rolls of the y axis with wavevector $\vec{k} = (k, 0)$ or of the x axis with wavevector $\vec{k} = (0, k)$; they can be square patterns with wavevector $\vec{k} = \sqrt{2}(k, k)/2$ or hexagonal patterns with a more complex combination of wavenumbers k_x and k_y such that the velocity and temperature fields must be invariant for rotation by $\pi/3$ about the origin and they must be periodic in the x- and y-directions [23]. Nonlinear stability analysis shows that for Rayleigh–Bénard convection, square patterns are not stable while rolls and hexagons are stable [28,29]. The Lorentz force due to the magnetic field breaks this invariance. Here, we have assumed that the perturbations are two-dimensional, i.e., $k_y = 0$, so that we have $\hat{u} = -d\hat{\psi}/dz, \hat{w} = ik\hat{\psi}$. We first present results the threshold Ra_c and critical wavenumber k_c of thermal convection for different values of Bi and the eigenfunctions $\hat{\theta}(z), \hat{\psi}(z)$ in the absence of the magnetic field, and then we analyze the effect of the magnetic field (i.e., of Ha) on the critical parameters (Ra_c, k_c) of the convection induced by Joule heating.

3.1. Threshold of Internal Heating-Induced Convection

We have computed the marginal stability curves for free-slip and no-slip boundary conditions and for different values of the Biot number Bi (Figure 3). The critical modes are stationary, i.e., $s_r = 0, s_i = 0$ and they are independent of Pr. The threshold of Joule heating-induced convection between two horizontal plates is lower than the one of the classic Rayleigh–Bénard convection with a constant temperature gradient between the

plates. This is due to the quadratic profile of the temperature field of the conduction state. We recover the results of previous studies [11–13,17].

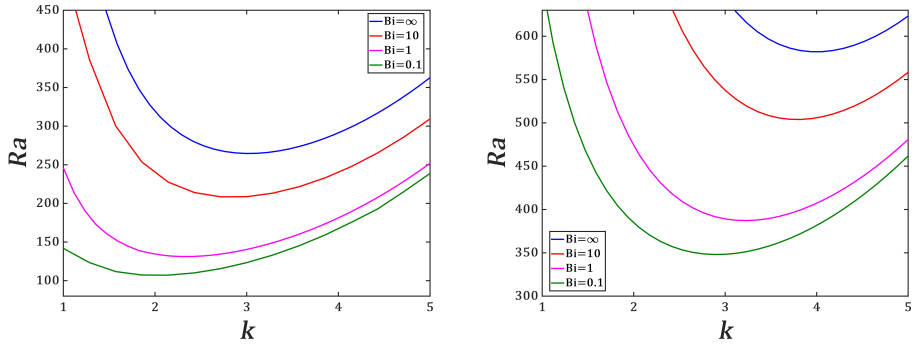


Figure 3. Stability curves for $s_r = 0$ in the plane (k, Ra) (**a**) free-slip and (**b**) no-slip boundary condition.

Table 2 presents the critical parameters (k_c, Ra_c) for chosen values of Bi. For $Bi \to \infty$ corresponding to isothermal boundary conditions, the threshold is the highest for both types of kinematic boundary conditions. This suggests that the heat exchange between the liquid layer and the environment favors the occurrence of Joule heating-induced convection. The effect of the Biot number on the size of thermoconvective cells induced by internal heating is significant: thermoconvective cells have a smaller size for isothermal boundary conditions than in the presence of heat exchange with the environment. For a fixed value of Bi, we recover the result that the free-slip conditions favor the convection as in the case of the classic Rayleigh–Bénard convection. In Figure 4, we have plotted the vertical profiles of the temperature perturbation $\hat{\theta}(z)$ and of the vertical velocity component $\hat{w}(z)$.

Table 2. Critical values for thermal convection induced due to internal heating for (**a**) free-slip and (**b**) no-slip boundary conditions.

Bi	Ra_c	k_c
	(**a**)	
∞	265.5	3.027
10	208	2.857
1	131.15	2.344
0.1	106.75	2.008
	(**b**)	
∞	583.20	3.998
10	503.85	3.784
1	387.2	3.246
0.1	348.0	2.902

The vertical profile of the temperature $\hat{\theta}(z)$ and of the vertical velocity component $\hat{w}(z)$ in Figure 4 show that the temperature and velocity perturbations perturbations penetrate into the lower stable part of the liquid. However, the upper part of the liquid layer is more active than the lower part as the last one is thermally stable. The eigenfunctions of the temperature field to which we have superimposed the velocity vectors and the stream functions $\psi(x, z) = const$ of the critical states are plotted in Figure 5. The cores of the stream functions are also located in the thermally unstable zone of the liquid layer.

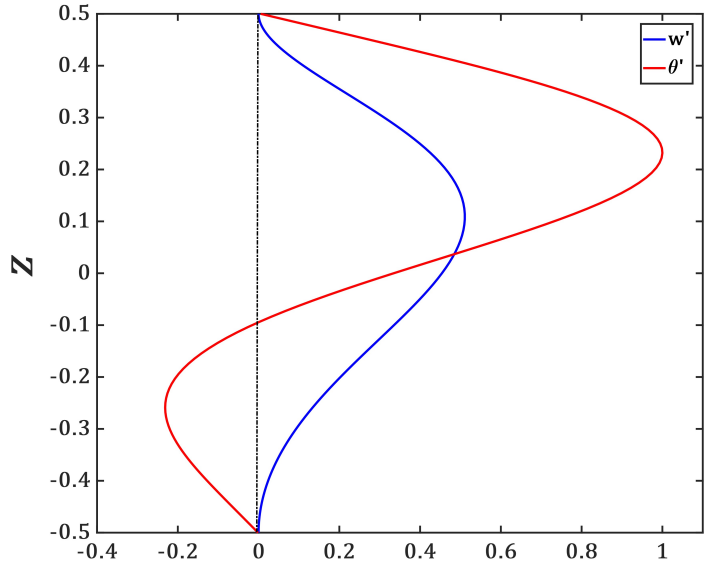


Figure 4. Profiles of the temperature perturbation $\hat{\theta}(z)$ and the axial velocity $\hat{w}(z)$ for isothermal no-slip condition $Bi = \infty$ in the absence of the magnetic field ($Ha = 0$).

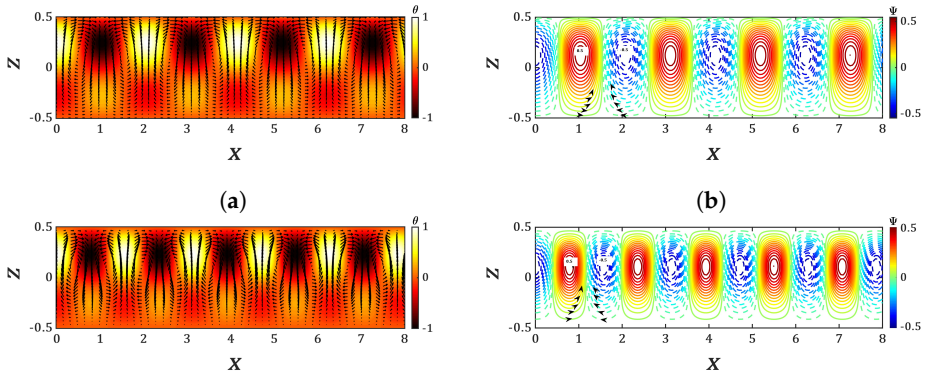


Figure 5. Isotherms and stream functions for isothermal boundaries ($Bi \to \infty$): (**a**,**b**) for free-slip boundary conditions and (**c**,**d**) for no-slip boundary conditions. Yellow and black zones in (**a**,**c**) correspond to hot and cold zones, respectively. Red color and blue color in (**b**,**d**) correspond to anticlockwise and clockwise vortices, respectively. Black arrows indicate the vortices' orientation.

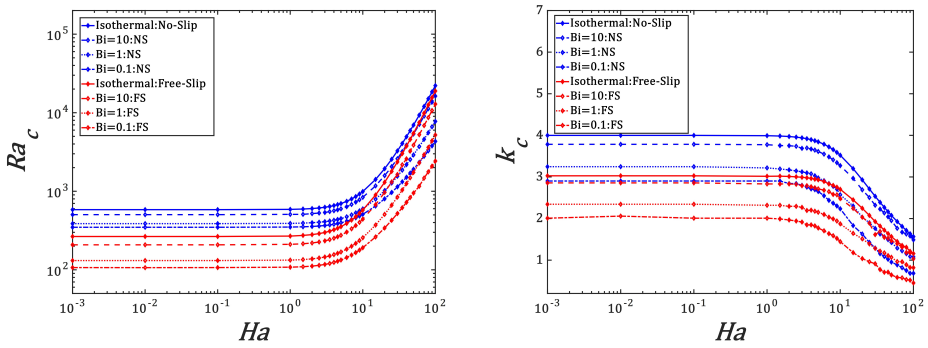
3.2. Effect of the Magnetic Field on Internal Heating Induced Convection

Different studies on thermal convection have shown that the vertical magnetic field delays the occurrence of the Rayleigh–Bénard convection with a decrease in cell size [23]. In the present study, we analyze the effect of the horizontal dimensionless magnetic field $\vec{B} = (1, 0, 0)$ on the threshold of internal heating-driven convection. We have solved the eigenvalue problem for different values of the Hartmann number Ha and plotted in Figure 6 the critical parameters (Ra_c, k_c) as functions of Ha. The critical modes are stationary for all values of Ha and the threshold is independent of Pr. The effect of the magnetic field on the threshold of thermal convection induced by Joule heating becomes significant for $Ha > 1$ where the threshold Ra_c and the critical wavelength $(\sim 1/k_c)$ start to increase for all values of the Biot number Bi. For both types of kinematic boundary conditions with imposed isothermal boundaries, the variations $Ra_c(Ha)$ can be approximated by quadratic polynomials. For free-slip boundary conditions,

$$Ra_c = 1.649Ha^2 + 22.12Ha + 222.6 \tag{24}$$

For no-slip boundary conditions,

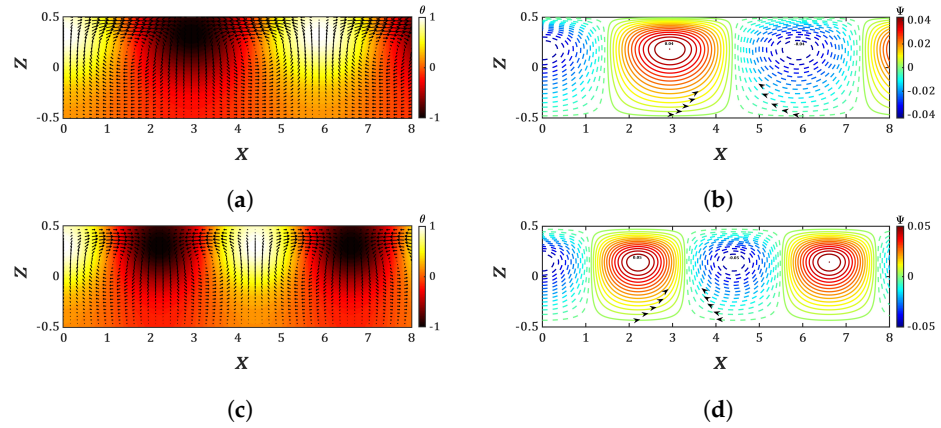
$$Ra_c = 1.771Ha^2 + 39.9Ha + 493.7 \tag{25}$$



(**a**) (**b**)

Figure 6. (**a**) Variation of Ra_c as a function of Ha for different boundary conditions and (**b**) variation of the critical wave number.

The stabilization effect of the magnetic field on thermal convection becomes significant when the applied field B_0 becomes larger than the characteristic intrinsic magnetic field B_i which depends on the properties and of the thickness of the liquid according to the relation (12). The isotherms and stream functions of the critical modes for $Bi = 1, Ha = 50$ are plotted in Figure 7. They illustrate the increase in the wavelength of the thermoconvective cells compared to the case without the magnetic field shown in Figure 5.



(**a**) (**b**)

(**c**) (**d**)

Figure 7. Isotherms and stream functions for $Bi = 1$ and $Ha = 50$: (**a**,**b**) for free-slip boundary conditions and (**c**,**d**) for no-slip boundary conditions. Yellow and black zones in (**a**,**c**) correspond to hot and cold zones, respectively. Red color and blue color in (**b**,**d**) correspond to anticlockwise and clockwise vortices, respectively. Black arrows indicate the vortices' orientation.

4. Discussion

We have revisited the linear stability of thermal convection induced by Joule heating in a liquid layer crossed by a homogeneous current of intensity I and bounded by two infinite horizontal plates that exchange heat with the environment. We have confirmed the results from previous studies [11–13,17] which have shown that the heat exchange between the liquid and the environment favors the appearance of thermal convection by the energy input into the liquid.

We have neglected the induced currents and magnetic fields in the liquid. The applied horizontal magnetic field delays the occurrence of thermal convection as in the case of Rayleigh-Bénard convection. In order to explain this result, we have derived from the system of Equation (14), the equation of the energy budget of the perturbations

$$\frac{dK}{dt} = B + D + L \tag{26}$$

where $K = \int \vec{u}^2 d^3\vec{r}$ is the kinetic energy, $B = \int w\theta' d^3\vec{r}$ is the power of the Archimedean buoyancy, $D = \sqrt{\frac{Pr}{Ra}} \int \left(\vec{u}.\nabla^2\vec{u}\right) d^3\vec{r} < 0$ [30] is the dissipation due to viscosity and $L = -Ha^2\sqrt{\frac{Pr}{Ra}} \int \left(v^2 + w^2\right) d^3\vec{r} < 0$ is the power performed by the Lorentz force in which we have neglected the power produced by the perturbation of the electric field. The Lorentz force contributes to the dissipation of the kinetic energy of the perturbations and thus, it delays the thermal convection.

Molten salts are used in some microfluidic systems used in aeronautics and in electronic circuitries [31]. They also have found a new application in the design of liquid metal batteries which consist of three superimposed liquid layers where an electrolyte is sandwiched between two liquid metals serving as electrodes [10,32]. These liquid layers are crossed by an electric current which induces a Joule heating in the electrolyte because of its low electrical conductivity compared to the liquid metals. To control the thermoconvective motion in liquid metal batteries where this motion can induce short-circuit and then damage the battery, the application of the magnetic field in the appropriate direction seems to be a solution to suppress or delay the thermoconvective motion in the battery.

From the critical values Ra_c, one can estimate the critical current J_{0c} required to trigger thermal convection induced by Joule heating in a liquid layer of thickness d using the relation (7) between the control parameter Ra and the applied current J:

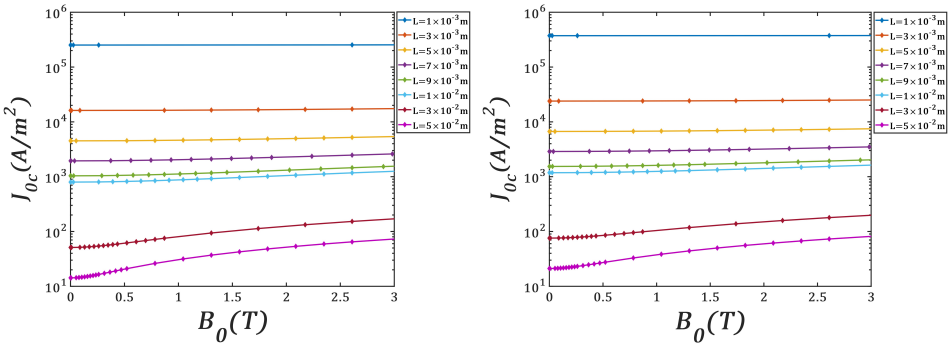
$$J = 8\sqrt{\frac{\sigma\lambda\nu\kappa Ra}{\alpha g d^5}} \tag{27}$$

Table 3 yields the values of the critical current J_c for a thickness $d = 10^{-2}$ m of the $LiCl - KCl$ molten salt with properties [7] : $\alpha = 2.93 \times 10^{-4}$ (1/K), $\lambda = 0.42$ (W/mK), $\sigma = 170$ (S/m), $\nu = 0.71 \times 10^{-6}$ (m^2/s), $\kappa = 2012 \times 10^{-7}$ (m^2/s).

Table 3. Critical value of current density to trigger convection for $d = 10^{-2}$ m.

	Ra_c	J_c (A/m^2)
No-slip	583.207	1184.10
Free-slip	265.505	799.06

Figure 8 shows the variation of critical current density J_{0c} that has to be applied to avoid convective motions as a function of the applied magnetic field B_0. These calculations have been made for different thicknesses of the molten salt layer.



(**a**) (**b**)

Figure 8. Variation of the critical current density J_{0c} as a function of applied horizontal magnetic field B_0 for different layer thickness, isothermal boundaries: (**a**) free-slip boundary and (**b**) no-slip boundary.

5. Conclusions

Thermal convection induced in a liquid layer confined between two infinite horizontal plates and subject to Joule heating by a homogeneous current has been revisited for different kinematic and thermal boundary conditions. The application of the horizontal magnetic field leads to the delay of thermal convection and to the increase in the wavelength of the thermoconvective cells. The energy budget shows that the Lorentz force produces a negative power and so it contributes, together with viscous forces, to the dissipation of the kinetic energy of thermoconvective perturbations induced by Joule heating in the liquid layer.

Author Contributions: Methodology, A.M.H., H.N.Y. and I.M.; Software, A.M.H., H.N.Y. and I.M.; Validation, A.M.H., H.N.Y. and I.M.; Formal analysis, A.M.H., H.N.Y. and I.M.; Investigation, A.M.H., H.N.Y. and I.M.; Resources, H.N.Y. and I.M.; Data curation, A.M.H., H.N.Y. and I.M.; Writing—original draft, A.M.H., H.N.Y. and I.M.; Writing—review & editing, H.N.Y. and I.M.; Supervision, H.N.Y. and I.M.; Project administration, I.M.; Funding acquisition, I.M. All authors have read and agreed to the published version of the manuscript.

Funding: This research was funded by French National Research Agency (ANR) through the Program Investissements d'Avenir (Grant ANR-10 LABX-09-01, LabEx EMC^3/project HILIMBA) and Région Normandie (Réseau d'Intérêt Normand—Label d'Excellence).

Data Availability Statement: The data will be made available by the authors on request.

Conflicts of Interest: The authors declare no conflicts of interest.

References

1. Kuchibhotla, A.; Banerjee, D.; Dhir, V. Forced convection heat transfer of molten Salts: A review. *Nucl. Eng. Des.* **2020**, *362*, 110591. [CrossRef]
2. Jeong, Y.S.; Seo, S.B.; Bang, I.C. Natural convection heat transfer characteristics of molten salt with internal heat generation. *J. Therm. Sci.* **2018**, *129*, 181–192. [CrossRef]
3. Zhang, S.; Sun, X.; Domniguez-Ontiveros, E.E. Numerical study on convective heat transfer and friction characteristics of molten salts in circular tubes. *Ann. Nucl. Energy* **2020**, *142*, 107375. [CrossRef]
4. Fiorina, C.; Cammi, A.; Luzzi, L.; Mikityuk, K.; Ninokata, H.; Ricotti, M.E. Thermal-hydraulics of internally heated molten salts and application to the Molten Salt Fast Reactor. *J. Phys. Conf. Ser.* **2014**, *501*, 012030. [CrossRef]
5. Nunes, V.M.B.; Queirós, C.S.; Lourenço, M.J.V.; Santos, F.J.V.; De castro, C.A.N. Molten salts as engineering fluids—A review: Part I. Molten alkali nitrates. *Appl. Energy* **2016**, *183*, 603–611. [CrossRef]
6. Turchi, C.S.; Vidal, J.; Bauer, M. Molten salt power towers operating at 600–650 C: Salt selection and cost benefits. *Sol. Energy* **2018**, *164*, 38–46. [CrossRef]
7. Shen, Y.; Zikanov, O. Thermal convection in a liquid metal battery. *Theor. Comput. Fluid Dyn.* **2016**, *30*, 275–294. [CrossRef]
8. Köllner, T.; Boeck, T.; Schumacher, J. Thermal Rayleigh-Marangoni convection in a three-layer liquid-metal-battery model. *Phys. Rev. E* **2017**, *95*, 053114. [CrossRef]

9. Personnettaz, P.; Beckstein, P.; Landgraf, S.; Köllner, T.; Nimtz, M.; Weber, N.; Weier, T. Thermally driven convection in Li||Bi liquid metal batteries. *J. Power Sources* **2018**, *401*, 362–374. [CrossRef]
10. Kelley, D.H.; Weier, T. Fluid Mechanics of Liquid Metal Batteries. *Appl. Mech. Rev.* **2018**, *70*, 020801. [CrossRef]
11. Sparrow, E.M.; Goldstein, R.J.; Jonsson, V. Thermal instability in a horizontal fluid layer: Effect of boundary conditions and non-linear temperature profile. *J. Fluid Mech.* **1964**, *18*, 513–528. [CrossRef]
12. Kulacki, F.A.; Goldstein, R.J. Thermal convection in a horizontal fluid layer with uniform volumetric energy sources. *J. Fluid Mech.* **1972**, *55*, 271–287. [CrossRef]
13. Kulacki, F.A.; Goldstein, R.J. Hydrodynamic instability in fluid layers with uniform volumetric energy sources. *Appl. Sci. Res.* **1972**, *31*, 81–109. [CrossRef]
14. Goluskin, D.; Spiegel, E.A. Convection driven by internal heating. *Phys. Lett. A* **2012**, *377*, 83–92. [CrossRef]
15. Goluskin, D. Internally heated convection beneath a poor conductor. *J. Fluid Mech.* **2015**, *771*, 36–56. [CrossRef]
16. Goluskin, D.; der Poel, E.P.V. Penetrative internally heated convection in two and three dimensions. *J. Fluid Mech.* **2016**, *791*, R6. [CrossRef]
17. Strauss, J.M. Penetrative convection in a layer of fluid heated from within. *Astrophys. J.* **1976**, *209*, 179–189. [CrossRef]
18. Yoshikawa, H.N.; Kang, C.; Mutabazi, I.; Zaussinger, F.; Haun, P.; Egbers, C. Thermoelectrohydrodynamic convection in parallel plate capacitors under dielectric heating conditions. *Phys. Rev. Fluids* **2020**, *5*, 113503. [CrossRef]
19. Mng'ang'a, J.; Onyango, E.R.; Chilingo, K.J. Joule heating and induced magnetic field on magnetohydrodynamic generalized Couette flow of Jeffrey fluid in an inclinded channel with Soret and Dufour effects. *Int. J. Ambient. Energy* **2024**, *45*, 2305328. [CrossRef]
20. Muhammad, M.Y.; Lawan, M.A.; Gambo, Y.Y. Heat absorption effect of magneto-natural convection flow in a vertical concentric annulus with influence of radial and induced magnetic field. *Sci. Rep.* **2024**, *14*, 15165.
21. Guidotti, R.A.; Masset, P. Thermally activated ("thermal")battery technology. Part I: An overview. *J. Power Sources* **2006**, *161*, 1443–1449. [CrossRef]
22. Masset, P.; Guidotti, R.A. Thermally activated ("thermal")battery technology. Part II: Molten salts electrolytes. *J. Power Sources* **2007**, *164*, 397–414. [CrossRef]
23. Chandrasekhar, S. *Hydrodynamic and Hydromagnetic Stability*; Oxford University Press: Oxford, UK, 1961.
24. Mutabazi, I.; Wesfreid, J.E.; Guyon, E. *Dynamics of Spatio-Temporal Cellular Structures: Henri Bénard centenary Review*; Springer: Berlin/Heidelberg, Germany, 2006.
25. Wang, Q.; Lohse, D.; Shishkina, O. Scaling in internally heated convection: A unifying theory. *Geophys. Res. Lett.* **2020**, *10*, 1029. [CrossRef]
26. Aurnou, J.M.; Olson, P.L. Experiments on Rayleigh–Bénard convection, magnetoconvection and rotating magnetoconvection in liquid gallium. *J. Fluid Mech.* **2001**, *430*, 283–307. [CrossRef]
27. Davidson, P.A. *An Introduction to Magnetohydrodynamics*; Cambridge University Press: Cambridge, UK, 2001.
28. Busse, F.H. Non-linear properties of thermal convection. *Rep. Prog. Phys.* **1978**, *41*, 1929–1967. [CrossRef]
29. Manneville, P. *Dissipative Structures and Weak Turbulence*; Academic Press: Cambridge, MA, USA, 1990.
30. Eckhardt, B.; Grossmann, S.; Lohse, D. Torque scaling in turbulent Taylor–Couette flow between independently rotating cylinders. *J. Fluid Mech.* **2007**, *581*, 221–250. [CrossRef]
31. Caraballo, A.; Galán-Casado, S.; Caballero, A.; Serena, S. Molten salts for sensible thermal energy storage: A review and an energy performance analysis. *Energies* **2021**, *14*, 1197. [CrossRef]
32. Kim, H.; Boysen, D.A.; Newhouse, J.M.; Spatocco, B.L.; Chung, B.; Burke, P.J.; Bradwell, D.J.; Jiang, K.; Tomaszowska, A.A.; Wang, K.; et al. Liquid Metal Batteries: Past, Present, and Future. *Chem. Rev.* **2013**, *113*, 2075–2099. [CrossRef]

Disclaimer/Publisher's Note: The statements, opinions and data contained in all publications are solely those of the individual author(s) and contributor(s) and not of MDPI and/or the editor(s). MDPI and/or the editor(s) disclaim responsibility for any injury to people or property resulting from any ideas, methods, instructions or products referred to in the content.